Structural Engineering and Mechanics, Vol. 31, No. 5 (2009) 567-585
DOI: http://dx.doi.org/10.12989/sem.2009.31.5.567

Flexural behavior of reinforced concrete beams strengthened with a hybrid inorganic matrix - steel fiber retrofit system

Christos G. Papakonstantinou† and Konstantinos Katakalos

University of Massachusetts Dartmouth, Department of Civil and Environmental Engineering
285 Old Westport Road, North Dartmouth, MA 02747, USA

(Received June 5, 2008, Accepted March 2, 2009)

Abstract. The aim of this study was to investigate the flexural behavior of reinforced concrete beams strengthened with a novel strengthening system. Concrete beams were strengthened with a hybrid retrofit system consisting of high strength steel cords impregnated in an inorganic fireproof matrix (Geopolymer). The strengthened reinforced concrete beams along with non-strengthened control beams were tested monotonically under four point bending loading conditions. Moreover, an analytical model is introduced, that can be used to analyze the flexural performance of the strengthened beams. The experimental results indicate that the failure of the strengthened beams was based on the yielding of the reinforcement in the tension face of the beams, followed by a local slippage of the steel cords. The flexural stiffness of the strengthened beams was significantly improved compared to the stiffness of the non-strengthened beams. In conclusion, the strengthening system can provide an effective alternative to commercially available systems.

Keywords: reinforced concrete; Steel Reinforced Polymers (SRP); inorganic resin; flexure; beams; strengthening system.

1. Introduction

Fiber reinforced polymer (FRP) composite materials encompass a wide variety of engineered materials that are designed to add strength where needed and reduce the weight of the structures. Advantages of FRP composites include high strength to weight ratios, corrosion resistance, electrical insulation, radio and magnetic transparency and ease of installation and construction.

Fiber reinforced polymer composite materials consist of high performance fibers embedded in a polymer matrix. The matrix serves to provide continuity to the composite, distribute applied loads between fibers, support the slender fibers against buckling, and protect the fibers from physical and environmental damage. For typical structural applications, fibers may take the form of a continuous unidirectional mat (also known as tow sheet), stitched or woven fabrics having single or multiple fiber orientation, or mats of chopped fiber having random orientation. The polymer matrix is typically an epoxy, vinyl ester, or polyester resin. Normally, only the material properties and orientations of the fibers are considered in determining the properties of the composite FRP.

† Associate Professor, Corresponding author, E-mail: cpapakonstan@umassd.edu

Table 1 Basic material properties of glass, carbon, aramid and steel fibers

	E-Glass	Carbon	Aramid	High Strength Steel
Tensile strength (MPa)	1300-3400	2000-5600	2500-3620	1000-2200
Modulus of elasticity (GPa)	22-62	150-325	48-76	185-200
Elongation (mm/mm)	0.03-0. 5	0.01-0.015	0.02-0.036	0.04
Coefficient of thermal expansion (10^{-6}m/m/^{o}K)	5.5	0.0	-0.5	6.5
Melting Point (^{o}C)	1100	310	420	1300
Density (gr/cm^{3})	2.5-2.6	1.7	1.4	7.9

There are three different types of fibers traditionally used in Civil engineering applications: E-glass, carbon and aramid (Kevlar). The raw fibers and the resulting composite materials exhibit an essentially linear stress-strain behavior to failure. The basic material properties of E-glass, carbon, and aramid fibers are provided in Table 1. These properties are contrasted with those of high strength steel such as that used for prestressing strands.

High strength composites made of carbon fibers and organic polymers are being successfully used for various types of repair applications. Several researchers have investigated the flexural capacity of strengthened beams (Grace and Abdel-Sayed 1996, Nanni 1997, Masmoudi *et al*. 1998, Shahawy and Beitelman 1999, Bonacci and Maalej 2001, Papakonstantinou *et al*. 2001b, Papakonstantinou *et al*. 2002b, Karayannis and Chalioris 2003), columns (Nanni 1993, Nanni and Gold 1998, Triantafillou and Antonopoulos 2000, Youm *et al*. 2006), beam-column joints (Mirmiran *et al*. 1999, Tsonos 2002, Tsonos 2004, Tsonos 2007). Their advantages include but are not limited to: high strength, light weight and resistance to corrosion. However, they are susceptible to fire and in some cases they degrade under UV radiation. Furthermore they are not environmental friendly (Lyon *et al*. 1997). A new inorganic fireproof matrix based on Geopolymers can be used instead of the traditional organic polymer resins. This fireproof, water-based, environmentally friendly matrix was initially evaluated for use in aircrafts and the infrastructure (Foden *et al*. 1997, Lyon *et al*. 1997, Balaguru and Kurtz 1998, Garon *et al*. 2000, Giancaspro *et al*. 2001, Papakonstantinou *et al*. 2001a, Giancaspro *et al*. 2002, Papakonstantinou *et al*. 2002a, Toutanji *et al*. 2002, Giancaspro *et al*. 2004, Papakonstantinou and Balaguru 2006, Papakonstantinou and Balaguru 2007a). Results from previous research studies have shown that resins based on Geopolymer are less permeable than concrete, thus slowing the flow of water through the weakened exterior surfaces (Balaguru 2003, Papakonstantinou and Balaguru 2007b). Vapor pressure is released because the matrices do not form a film. The matrix contains nano-scale silica particles and hardeners. These nano-particles penetrate and close small cracks on the concrete surface (Balaguru and Kurtz 1998). In strengthening applications, the matrices form a strong bond between the surface of the concrete and the fiber reinforcement (Kurtz and Balaguru 2001, Papakonstantinou and Balaguru 2007b). This study utilizes the Geopolymer resin in combination with high strength steel cords for strengthening reinforced concrete beams.

Tapes made with high strength steel fibers have been used either with cementitious grouts (SRG), or with organic resins (SRP) by several researchers (Wobbe *et al*. 2004, Barton *et al*. 2005, Casadei *et al*. 2005a, Casadei *et al*. 2005b, Huang *et al*. 2005, Harrison *et al*. 2006, Pecce *et al*. 2006, Prota *et al*. 2006, Ceroni and Pecce 2007, Lopez *et al*. 2007). It was shown that the addition of these strengthening systems could be an effective alternative for repairs and retrofit of reinforced concrete structural elements. The SRP is relatively lightweight in comparison to steel plates and is more

ductile than the carbon, glass or aramid fibers. In all published studies the mode of failure was based on the delamination of the SRP (Wobbe *et al*. 2004, Barton *et al*. 2005, Casadei *et al*. 2005a, Casadei *et al*. 2005b, Huang *et al*. 2005, Kim *et al*. 2005, Harrison *et al*. 2006, Pecce *et al*. 2006, Prota *et al*. 2006, Ceroni and Pecce 2007, Lopez *et al*. 2007), which resembles the most common mode of failure in beams strengthened with typical FRP systems based on organic resins (Nanni 1993, Sharif *et al*. 1994, Arduini *et al*. 1997, Saadatmanesh and Malek 1998, Shahawy and Beitelman 1999). The most commonly used steel tapes are made using ultra high strength steel fibers coated with brass. According to the manufacturer, the fibers have tensile strength that can reach eleven times the strength of regular reinforcing steel bars, while the brass coating has a specific chemical composition that ensures a good bond with organic resins (Wobbe *et al*. 2004).

This study deals with a hybrid strengthening system, which is quite similar to the SRG found in the literature (Barton *et al*. 2005, Kim *et al*. 2005, Pecce *et al*. 2006). The strengthening system consists of a new type steel fiber tape impregnated in a fireproof inorganic (Geopolymer) matrix. The steel tapes used in this study were fabricated specifically for this research program. The main differences between the commercially available steel tapes and the steel tapes used in this study are that: (i) the geometry of the steel cords that are used in the tape is different: cords in this study consist of a larger number but smaller diameter wires compared to the commercially available cords, and (ii) the steel wires were coated with Zinc instead of Brass. To the best of the author's knowledge, this is the first time that a steel fiber based strengthening system was used with a Geopolymer matrix.

In addition to the presentation and discussion of the experimental results, an analytical model was developed for the prediction of the flexural behavior of strengthened reinforced beams and is also presented in this paper.

2. Experimental program

2.1 Beam details and instrumentation

A total of five reinforced concrete beams were tested. The first two were not externally strengthened and were used as control beams (CB1 and CB2), in order to evaluate the efficiency of the retrofit scheme. The remaining three reinforced concrete beams were externally strengthened with single directional steel reinforced inorganic polymers. One strengthened beam (RB1) was strengthened using 90 steel cords, while the remaining two (RB2 and RB3) were strengthened using 35 steel cords. The difference between beams RB2 and RB3 was the thickness of the matrix used for the application of the steel cords (see Table 2).

The geometry and the reinforcement of the simply supported reinforced concrete specimens are illustrated in Fig. 1. The beams were 100 mm wide, 150 mm deep, while their length was 1220 mm. All beams were reinforced longitudinally with four plain bars, each having a diameter of 6 mm. Two bars were placed on the tension and two on the compression face of the beam. The effective depth was 130 mm. The beams were reinforced with 6 mm double leg open stirrups spaced evenly at 63 mm. The beams were designed based on the ACI-318 design code so that a shear failure will be avoided in all cases (even with the addition of the strengthening system). The details of the beams are provided in Table 2. Prior to the fabrication of the beams, strain gages were installed at the midpoint of the tensile steel of all specimens (Fig. 1).

Table 2 Specimen details

Beam	No of cords	Total strength of SRP (kN)	Reinforcing bars in tension face	Matrix		
				Type	Thickness	Curing Time
CB-1	0	N/A	2Ø6	none	none	none
CB-2	0	N/A	2Ø6	none	none	none
RB-1	90	72	2Ø6	Inorganic	2 mm	14 days
RB-2	35	28	2Ø6	Inorganic	2 mm	30 days
RB-3	35	28	2Ø6	Inorganic	3 mm	30 days

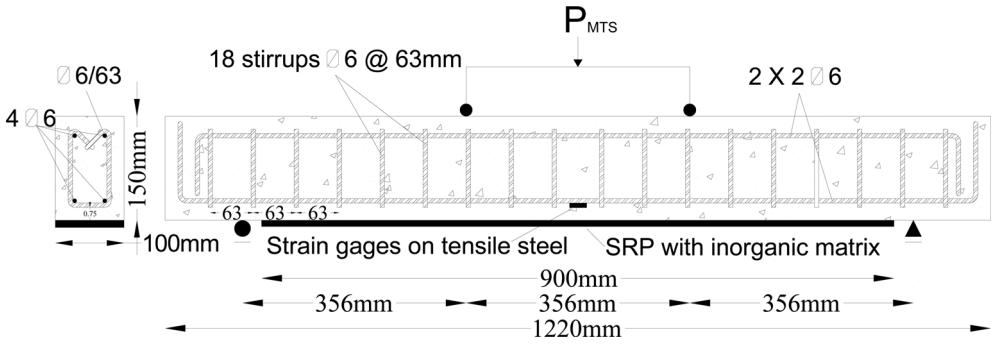

Fig. 1 Specimen details

All beams were kept in a wet curing room for a minimum of 28 days. Before the application of the SRP the bottom surface of the beams was grinded with an angle grinder to remove all laitance and dirt from the surface. The concrete surface was then cleaned with a steel wire brush, and finally compressed air was used to remove concrete dust and dirt that had settled on the beam. This ensured that the concrete surface was clean of contaminants and debris.

The Geopolymer resin was prepared by mixing an aqueous solution containing silica and potassium oxide, with silica powder. In addition, water and wetting agent were added to produce a resin with an initial viscosity of about 0.6 N s/m^2. The components were mixed using a small high shear mixer for two minutes. An initial thin layer (of approximately 0.5 mm) of the matrix was applied to the concrete surface using a roller. The SRP tape was then applied to the primed surface, followed by a second layer of matrix. A grooved roller was used to press the SRP and remove all possible air pockets from the matrix. The strengthened beams were stored at room temperature for at least 14 days before testing.

2.2 Materials

A detailed description of the materials including their mechanical properties is provided in the following sections.

2.2.1 Concrete and steel reinforcement

The 28 day compressive strength was obtained using cylindrical specimens, and was 25 MPa. The steel reinforcement was made with undeformed round bars. The mechanical properties of the steel

reinforcement were experimentally determined. More specifically, the yield stress was equal to 530 MPa, the ultimate stress equal to 590 MPa, and the modulus of elasticity was 200 GPa. The stress strain curve exhibited an initial elastic region followed by a fully plastic region until fracture. The properties were determined using uniaxial tension tests performed in the laboratory. In order to ensure adequate development length all longitudinal reinforcing bars were bend 90^o at the ends of the beams (see Fig. 1).

2.2.2 Inorganic resin

The inorganic matrix known as Geopolymer is a low viscosity resin. It is prepared by mixing an aluminosilicate powder with a water based activator. At room temperatures it has a pot life of about 3 hours. The matrix was initially investigated for use in aircraft structures and was also modified for use as a coating material and adhesive for brick, concrete, wood, and steel. The cementitious part is a potassium aluminosilicate. The resin hardens to an amorphous (glassy) structure at moderate temperatures of 80^o to 150^{o}C. Hardeners have been developed to obtain room temperature cure in about a day. The research conducted so far has focused on the mechanical, thermal, and durability properties of composites made with carbon, glass, and steel (Hammell *et al*. 1998). The unique features of the matrix are as follows:

- The resin is prepared by mixing a liquid component with silica powder. Fillers and hardening agents can be added to the powder component. The two components can be mixed to a paint consistency.
- Since the matrix is water based, tools and spills can be cleaned with water. All of the components are nontoxic and no fumes are emitted during mixing or curing. The excess material, or material removed from the old application can be discarded as general waste.
- The pot life varies from 30 minutes to 3 hours for compositions that cure at room temperature. Compositions that require heat for curing at 80^o to 150^{o}C can be stored for weeks.
- Common application procedures such as brushing and spraying can be used for the application. The matrix bonds well with carbon and glass fibers, that can be used as reinforcements. Tows and fabrics made out of carbon and glass can also be attached to existing structures. (Hammell *et al*. 1998, Papakonstantinou *et al*. 2001a).
- The matrix can withstand temperatures up to 1000^{o}C and is not affected by UV radiation. Fire tests show that the flame-spread index is zero. Since the air permeability is low, the matrix also protects the material it is covering by reducing the amount of oxygen for combustion (Lyon *et al*. 1997).

2.2.3 Steel fibers

Two types of steel fiber tape were used. They consisted of either 90 or 35 steel cords. Each cord consists of 3 smaller cords, which are made using 7 smaller wires (each wire has a diameter of 0.15 mm) twisted together. It is similar to a prestressing strand but considerably smaller in size. The properties of each cord were obtained using uniaxial tension tests and are presented in Table 3. The

Table 3 Properties of the steel cords

	E_S (GPa)	Cord diameter (mm)	Number of filaments	Diameter of filament (mm)	ε_S (%)	Cord Break Strength (N)
Steel Cords	200	0.91	21	0.15	0.587	880

Fig. 2 Testing setup

stress strain curve obtained from the testing was bilinear (elastic – fully plastic), without any strain hardening region. Steel fibers were bonded at the tension face of the beams using the previously described inorganic matrix. The total length of the steel cords was 900 mm.

2.3 Testing procedure

All specimens were submitted to four-point monotonic bending over a 1068 mm span. The load was applied by steel beam bearing rockers placed at one-third span (356 mm from each end support). The experimental setup is shown in Fig. 2. To facilitate the testing setup, a steel beam setup was connected to a computer controlled MTS 250 kN top mounted hydraulic actuator. The experiments were conducted under displacement control using a loading rate of 3 mm/min.

Wooden plates were positioned at the loading points to distribute the load and avoid local crushing of concrete. Three LVDTs were used to measure the deflections of the beam. The first LVDT was measuring the average mid-span deflection at the tensile fiber. The remaining two LVDTs were positioned so that the deflections could be measured at midspan from the neutral axis. These LVDTs were placed one on each side of the beam. Moreover, the strains of the two tensile steel bars were recorded. The load was measured from a load cell, which was attached on the actuator. Displacements were also measured from the crosshead movement of the loading frame and were compared with the LVDT deflections. All measurements were recorded using a Vishay System 5000 Data Acquisition System.

3. Experimental results and discussion

The results discussed in the following sections focus on the load-deflection behavior, failure modes, crack patterns, strength increase and strains. Table 4. provides a summary of the experimental results.

Table 4 Summary of experimental and theoretical results

		At cracking		At yielding		At ultimate		Mode of failure	Ductility Ratio
		Exp.	Anal.	Exp.	Anal.	Exp.	Anal.		
CB1	Load (N)	7110	6863	11400	11270	23900	26500	Steel yielding	3.06
	Deflection (mm)	0.307	0.21	2.12	2.21	8.61	8.48		
	Strain (μstrain)[1]	700	1000	2200	2200	N/A[2]	8650		
CB2	Load (N)	6919	6863	12491	11270	23400	26500	Steel yielding	2.87
	Deflection (mm)	0.22	0.21	2.043	2.21	7.9	8.48		
	Strain (μstrain)[1]	N/A[2]	1000	2200	2200	N/A[2]	8650		
RB1	Load (N)	7080	6863	11200	16760	25800	54700	Steel yielding - Slippage of steel fibers	4.83
	Deflection (mm)	0.41	0.21	1.0	1.03	5.83	6.4		
	Strain (μstrain)[1]	515	800	2200	2200	N/A[2]	5700		
RB2	Load (N)	6995	6863	13040	14100	25200	35000	Steel yielding - Slippage of steel fibers	3.02
	Deflection (mm)	0.29	0.21	1.05	1.28	4.23	7.3		
	Strain (μstrain)[1]	380	800	2200	2200	N/A[2]	7100		
RB3	Load (N)	7220	6863	13500	14100	30500	35000	Steel yielding - Slippage of steel fibers	3.32
	Deflection (mm)	0.30	0.21	1.25	1.28	5.4	7.3		
	Strain (μstrain)[1]	395	800	2200	2200	N/A[2]	7100		

[1]Strain measured at tensile steel reinforcing bars.
[2]Not available since strain gages failed prematurely.

3.1 Ductility, failure modes and crack patterns

The control beams failed as typical under-reinforced beams: steel yielding followed by concrete crushing. Since the reinforcement ratio reinforcement used in this study was very low, no shear cracks were observed. Two or three major flexural cracks were initiated typically at the third points of the beams. The cracks propagated as the load increased and they opened significantly after the yielding of the steel reinforcement. The strengthened beams failed in a similar manner. The yielding of the rebar was followed by the failure of the SRP system. The relatively short curing time (14 days) was obviously not adequate for the complete cure of the matrix in beam RB1. All strengthened beams (RB1, RB2 and RB3) exhibited a quite similar mode of failure. After the yielding of the steel, the matrix cracked but the steel cords continued to carry load while bridging the crack. Before they reached their fracture strain (1.1%), the cords started to slip in the matrix. The slippage was in some cases sudden while in some other gradual. More specifically, in RB1 and RB2 the slippage started to occur even before the ultimate load was reached, while in RB3 the slippage occurred suddenly. The strain on the SRP at the initiation of the slippage was approximately 0.8%. In beam RB2 a local slippage of the fibers in the matrix was observed (Fig. 3), while in beams RB1 and RB3 the slippage was more pronounced and resulted in local delamination of the cords. The interface between the steel fibers and the inorganic matrix should be further evaluated. The authors believe that the zinc coating of the steel fibers might provide a possible explanation for this interfacial slippage. It should be noted that no delamination was observed

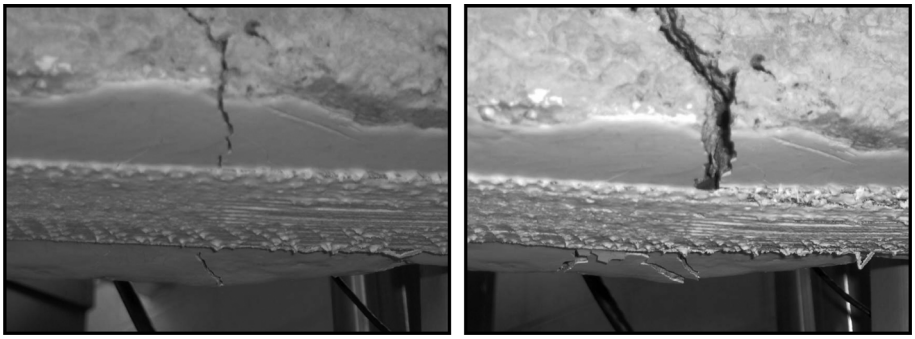

Fig. 3 Crack opening in tension face of beam RB-2 (a) post cracking (b) post yielding

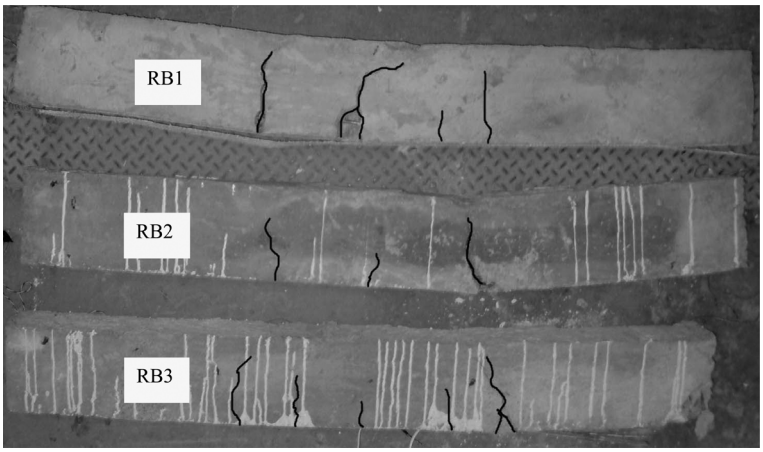

Fig. 4 Crack pattern in strengthened beams

between the concrete and the matrix. After the slippage, the load dropped and the flexural behavior of the strengthened beams became almost identical to that of the non-strengthened beam.

One of the most commonly used measures of ductility was adopted to numerically evaluate the ductility provided by the strengthening system. Most specifically the ratio of the post yield deformation to the yield deformation was used. The ductility ratios are shown in Table 4 and are approximately at the same level for the control and the strengthened beams. The yield point was defined in all cases by the recorded strain. Although the deformation at the ultimate load was lower for the strengthened beams, the total ductility of the beams was not affected by the strengthening system.

The crack pattern was similar for all beams (see Fig. 4). Only limited flexural cracks were observed exactly as in the control beams. The inorganic matrix is brittle, so when a crack forms in the reinforced concrete beam it eventually propagates through the inorganic matrix. The steel fibers at this point act similarly to steel reinforcement in a cracked concrete section. The inorganic matrix maintains the bond to the steel cords after cracking due to the phenomenon of local delamination: the steel cords remain bonded to the inorganic resin over only the uncracked segments. Therefore, the tensile stresses in the inorganic matrix as well as the interface between the matrix and the concrete remain at low levels. In comparison, cracks typically cannot go through the organic matrices (Kurtz and Balaguru 2001), and as a result the failures are typically based on the

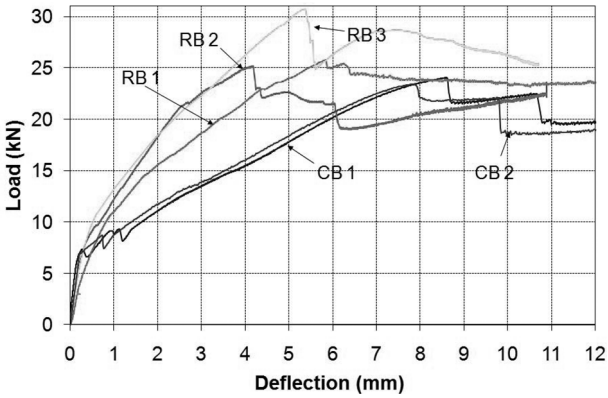

Fig. 5 Load deflection curves

delamination of the FRP or SRP system from the concrete substrate. The load-deflection curves of the tested beams are shown in Fig. 5. It is obvious that the strengthened beams exhibited higher strength and post cracking stiffness. The slippage of the cords resulted in a relatively gradual mode of failure for beam RB1. Furthermore, after the ultimate load was reached the behavior of the strengthened beams resembled the behavior of the control beam. In beam RB3 the failure was more notable than in RB2 and the ultimate load capacity was significantly improved. Since the only difference between these beams was the thickness of the SRP layer (amount of matrix), we can conclude that this was a result of matrix addition. The flexural strength was increased by 20% for beam RB3, while the increase was insignificant for the remaining two retrofitted beams (RB1 and RB2). As described before, the insufficient curing time and the thin layer of matrix did not help in reaching the expected capacity. The authors believe that the identified problems could be addressed in a future study.

3.2 Flexural stiffness

The flexural stiffness EI was computed for each beam in its post-crack and post-yield stages using the following equation

$$EI = \frac{P}{\Delta} \cdot \left(\frac{l/3}{24}\right) \cdot [3l^2 - 4(l/3)^2] \tag{1}$$

Where,

P = total load (kN), equal to the sum of the two point loads

Δ = midspan deflection (m), recorded at a load of P

l = span (m).

Eq. (1) is based on the assumptions that all materials behave linearly elastic and EI is constant. It is based on the equation for maximum elastic deflections of beams subjected to 4 point bending conditions. Since EI varies with location along the span, the computed flexural stiffness should be considered an average effective stiffness. For the post-crack data, the (P/Δ) term was calculated by identifying the crack point and the yield point on the load-deflection curve and then fitting a least-squares regression line between them. For the post-yield data, the (P/Δ) term was calculated by fitting a best-fit line through the linear portion of the post-yield curve.

Table 5 Comparison of stiffness increase

Beam	Post-Cracking					Post-Yielding			
	Total net steel fiber area (mm^2)	Flexural stiffness (kNm^2)	Flexural stiffness increase (kNm^2)	% increase	Flexural stiffness increase per steel fiber area (MN)	Flexural stiffness (kNm^2)	Flexural stiffness increase (kNm^2)	% increase	Flexural stiffness increase per steel fiber area (MN)
CB[1]	-	117.23	-	-	-	81.91	-	-	-
RB1	33.39	301.93	184.69	157	5531	130.70	48.7	59	1461
RB2	12.98	343.91	226.67	193	17455	165.34	83.43	102	6425
RB3	12.98	285.82	168.59	168	12982	177.12	95.21	116	7332
CB[2]	-	225.70	-	-	-	22.42	-	-	-
SRP30[2]	13.07	262.84	37.14	16	2841	101.95	79.53	355	6084
SRP60[2]	26.14	221.75	-3.95	-2	-151	108.82	86.40	385	3305
SRP 100[2]	43.57	277.19	51.49	23	1182	102.96	80.54	359	1849
SRP 100U[2]	43.57	322.19	96.49	43	2214	83.51	61.09	272	1402

[1]Average values from CB1 and CB2.
[2]Specimens reported by Kim *et al.* (2005).

Stiffness increase is quantified by subtracting the flexural stiffness of the respective control from the flexural stiffness of each strengthened beam. Differences in steel cord area were accounted for by using the equation

$$\text{Stiffness increase per unit steel fiber area} = \frac{\Delta EI}{A_{steel}} \tag{2}$$

Where,

ΔEI = flexural stiffness increase, with respect to the control beam ($kN\text{-}m^2$)

A_{steel} = SRP area (m^2)

The stiffness increases are presented in Table 5. For comparison purposes data provided by Kim *et al.* (2005) are also included in the table. Kim has used similar size reinforced concrete beams strengthened with SRP using an organic matrix (Sikadur resin). As it can be observed from Table 5, the post cracking increase exceeded 150% in all cases that the strengthening system was used. The increase is considerably higher than the increase reported from Kim (2005). The beams used in this study had significantly lower reinforcement ratio (ρ = 0.004) compared to beams used by Kim (ρ = 0.01). Another significant difference is that in the current study no shear cracks were observed. The inorganic matrix seems to be more efficient than the organic matrix used by Kim *et al.* (2005). Furthermore, the post yielding stiffness increases per steel fiber area are also higher for the beams strengthened with the inorganic matrix. An examination of the normalized flexural stiffness increase (flexural stiffness increase per unit steel fiber area) further supports the finding, that the use of the inorganic matrix is more efficient.

3.3 Analytical model for strengthened beams

An analytical model was developed to predict the flexural performance of strengthened reinforced

concrete beams. The model incorporates the contribution of the concrete in tension up to cracking, as well as actual stress strain behaviour of concrete in compression instead of the rectangular stress block suggested by ACI 318-05 (2005). We make the assumption that there is perfect bond between the steel fibers and the concrete, and that the failure in strengthened beams is dictated by the failure of the steel cords. For non strengthened beams we can assume that failure is a result of concrete crushing.

The reduced concrete's strength, f_c'', accounts for differences between cylinder strength and actual member strength, and is entered as

$$f_c'' = k \cdot f_c' \tag{3}$$

where,

f_c' is the compressive strength of concrete calculated from laboratory tests and

k is a constant taken equal to 0.92 (Hognestad 1951)

The modulus of elasticity of concrete was determined based on the following equation (ACI 318-05, 2005)

$$E_c(psi) = 4780 \cdot \sqrt{f_c'} \tag{4}$$

The calculations are based on strain compatibility, force equilibrium and moment equilibrium (Fig. 6).

To generate the moment-curvature curve, the strain in the extreme fiber of concrete, ε_{cm}, is increased until failure or 0.003 in increments of 0.0001 strain. The strains of steel rebar and steel fiber sheet can be calculated from ε_{cm} using

$$\varepsilon_{si} = \varepsilon_{cm}\frac{c - d_i}{c} \tag{5}$$

$$\varepsilon_f = \varepsilon_{cm}\frac{c - d_f}{c} \tag{6}$$

The variable c is the distance to the neutral axis and d is the depth from the top fiber of the concrete beam to the centroid of each material. The subscripts "*si*" and "*f*" are used to indicate steel and steel fiber properties respectively.

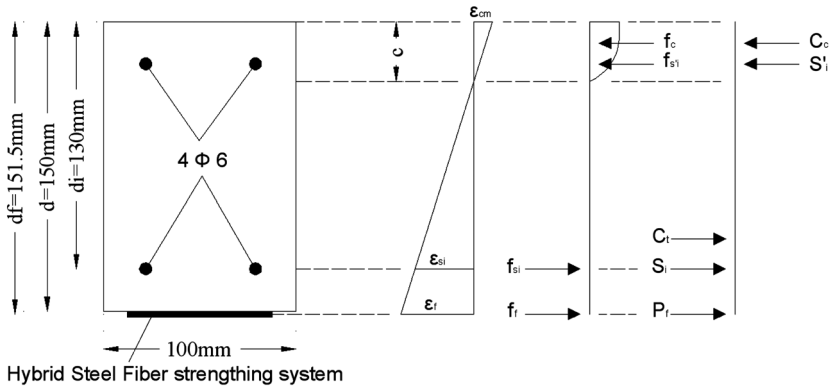

Fig. 6 Strain, stress, and force diagrams across depth of rectangular section

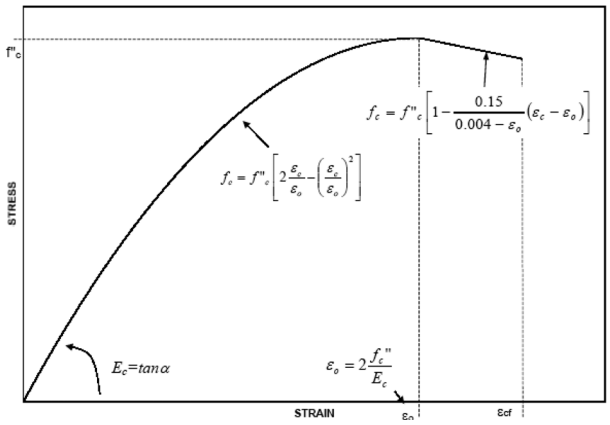

Fig. 7 Idealized stress-strain curve for concrete in uniaxial compression (Hognestad 1951)

The steel and fiber stresses are calculated from the stress strain curves of steel and fiber

$$f_{si} = E_s \cdot \varepsilon_{si}, \quad \text{if } \varepsilon_{si} \le \varepsilon_y$$
$$f_{si} = f_y, \quad \text{if } \varepsilon_{si} > \varepsilon_y \tag{7}$$

$$f_f = E_f \cdot \varepsilon_f \tag{8}$$

where the subscript "y" denotes the yielding of steel.

The forces from the steel and steel cord are then calculated by multiplying their stresses and areas.

$$S_i = f_{si} \cdot A_{si} \tag{9}$$

$$P_f = f_f \cdot A_f \tag{10}$$

The distribution of concrete stresses in the compression zone is derived from the stress-strain curve of concrete (Hognestad 1951). (Fig. 7) The concrete stresses in the compression zone can be evaluated using the following expressions

$$f_c = f_c'' \cdot \left[2\frac{\varepsilon_c}{\varepsilon_o} - \left(\frac{\varepsilon_c}{\varepsilon_o}\right)^2\right] \quad \text{if} \quad 0 \le \varepsilon_c \le \varepsilon_o \tag{11}$$

$$f_c = f_c'' \cdot \left[1 - \frac{0.15}{0.004 - \varepsilon_o}(\varepsilon_c - \varepsilon_o)\right] \quad \text{if} \quad \varepsilon_c \le \varepsilon_o \le 0.003 \tag{12}$$

Where: $\varepsilon_o = 2\frac{f_c''}{E_c}$

To calculate the concrete compression force C_c, a factor α is calculated from the relationship of A, the area under the stress strain curve of concrete. The factor α is being used to convert the concrete stress distribution into an equivalent rectangular stress distribution

$$A = \int_0^{e_{cn}} f_c d\varepsilon_c = af_c'' \varepsilon_{cm} \quad \text{or} \quad \alpha = \frac{\int_0^{e_{cn}} f_c d\varepsilon_c}{f_c'' \varepsilon_{cm}} \tag{13}$$

Using the calculated α

$$C_c = \alpha \cdot f_c'' \cdot b \cdot c \tag{14}$$

The position of the resultant concrete compressive force measured from the top concrete fiber is expressed in terms of a parameter γ

$$d_c = \gamma c \tag{15}$$

where γ is calculated from a relationship between the first moment of area under the stress-strain diagram about the origin and the strain at the centroid of area

$$\gamma = \frac{\int_0^{e_{cn}} \varepsilon_c f_c d\varepsilon_c}{\varepsilon_{cm} \cdot \int_0^{e_{cn}} f_c d\varepsilon_c} \tag{16}$$

The tensile strength of concrete before and after cracking was also included. After the formation of the first crack, the average stress in the concrete will be reduced and continue to decrease as further cracks develop. The tensile capacity of concrete after cracking is calculated using the relationship suggested by Vecchio and Collins (1986)

$$f_{ct} = \frac{\alpha_1 \cdot \alpha_2 \cdot f_{cr}}{1 + \sqrt{500 \varepsilon_m}} \quad \text{if} \quad \varepsilon_{cm} > \varepsilon_{cr} \tag{17}$$

where,

ε_{cr} is the strain of concrete at cracking, α_1 taken equal to 0.7 and α_2 equal to 1.0, are factors accounting for bond characteristics of reinforcement and for sustained or repeated loading respectively, f_{cr} is the stress when cracking occurs and f_{ct} is the tensile capacity of concrete after cracking

All internal forces are set to reach equilibrium and the necessary c, the location of the neutral axis for each of the incremental values of ε_{cm}, is calculated from

$$\alpha \cdot f_c'' \cdot b \cdot c + \sum_{i=1}^{n} f_{si} A_{si} + f_f A_f + f_{ct} b \frac{d-c}{2} = 0 \tag{18}$$

With the increments of ε_{cm} and the corresponding values of c found from equilibrium, summing the moments of these forces about an axis produces the internal resisting moment. This can be plotted with respect to the curvature at midspan, to produce the moment-curvature curve

$$M = \alpha \cdot f_c'' \cdot b \cdot c\left(\frac{h}{2} - \gamma c\right) + \sum_{i=1}^{n} f_{si} A_{si}\left(\frac{h}{2} - d_i\right) + f_f A_f\left(\frac{h}{2} - d_f\right) + f_{ct} b \frac{2(h-c)}{3} \frac{d-c}{2} \tag{19}$$

$$\phi = \frac{\varepsilon_{cm}}{c} \tag{20}$$

For the four point loading condition deflection can be calculated as

$$\Delta = \frac{23PL^3}{1296EI} \tag{21}$$

where a load of $P/2$ is applied at the two third points of the beam.

The internal moment in a beam under four point loading is calculated and substituted into the deflection equation to produce the deflection in terms of curvature

$$M = \frac{PL}{6} \tag{22}$$

Substituting this into the deflection equation

$$\Delta = \frac{23 \cdot 6ML^2}{1296EI} = \frac{\phi L^2}{9.39} \tag{23}$$

This analytical methodology can be used to determine the load vs. deflection behaviour of strengthened or non-strengthened reinforced concrete beams. The analytical results are compared with the experimental in Table 4. The load-deflection graphs shown in Fig. 8 include curves that were obtained using the suggested model. Curves for beam RB1 are not plotted, since as mentioned previously the experimental results were affected by the short curing time of the matrix. The analytical curve can be used for both RB2 and RB3 since the difference between the two is only 0.5 mm in depth d_f of the steel fibers. The maximum load for the strengthened beams was obtained assuming that the failure is a result of the steel cord fracture at a strain level of 1.1%. We can see that the theoretical ultimate load for beam RB3 was 35 kN while the experimental was 30.5 kN. Assuming a linear strain distribution and using the previously described model to calculate the strains at the ultimate levels, it was calculated that the slippage of the steel fibers in the matrix occurred at a strain of approximately 0.87%, which is lower than the fracture strain of the steel cords. It is obvious, that the proposed analytical model can predict the flexural behaviour of both strengthened and non strengthened reinforced concrete beams with good accuracy. Furthermore, the slopes of the load deflection curves can be determined with excellent accuracy. The main problem is

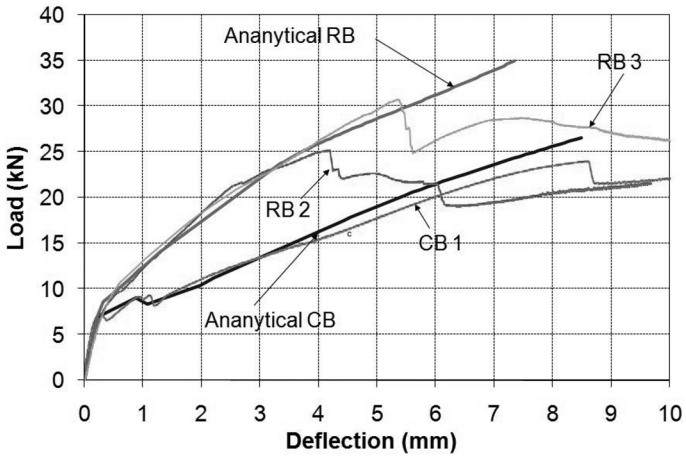

Fig. 8 Experimantal vs analytical load-deflection curves

the determination of the maximum flexural capacity. As mentioned previously, one can assume that the failure is dictated by the fracture of the steel fibers (strain of 1.1%). But since experimentally this was not the case, we could possibly use the model predicting failure when the slippage occurs (strain of 0.87%). This hypothesis might provide a solution to the problem, but in order to make a safe statement more experimental results are needed. The proposed model can be used for any type of reinforced concrete beam strengthened with externally bonded fiber reinforced polymers.

4. Conclusions

This study addressed the use of a hybrid retrofit system. The flexural performance of the strengthened beams has been identified using experimental and analytical investigations. The following conclusion can be drawn:

- Geopolymer matrix can be used for the fabrication of a novel strengthening system based on high strength steel cords
- The curing time of the matrix plays an extremely important role in the effectiveness of the system
- No delamination was observed between the matrix and the concrete substrate
- The mode of failure was based on the yielding of the reinforcement, followed by slippage of the SRP.
- The flexural stiffness of the strengthened reinforced concrete beams is significantly improved compared to non strengthened beams and beams strengthened with organic polymers.
- The proposed analytical model can predict with good accuracy the flexural behavior of strengthened reinforced concrete beams.

References

ACI 318-05 (2005), *Building Code Requirements for Structural Concrete and Commentary*, American Concrete Institute.

Arduini, M., Di Tommaso, A. and Nanni, A. (1997), "Brittle failure in FRP plate and sheet bonded beams", *ACI Struct. J.*, **94**(4), 363-370.

Balaguru, P. and Kurtz, S. (1998), "Use of inorganic polymer-fiber composites for repair and rehabilitation of infrastructures", Proceedings of the International Seminar on Repair and Rehabilitation of Reinforced Concrete Structures: The State of the Art, Maracaibo, Venezuela, 155-168.

Balaguru, P.N. (2003), "High strength composites for infrastructure: Current and future directions of research", International Society of Offshore and Polar Engineers, Honolulu, HI, United States, 2251-2259.

Barton, B., Wobbe, E., Dharani, L.R., Silva, P., Birman, V., Nanni, A., Alkhrdaji, T., Thomas, J. and Tunis, G. (2005), "Characterization of reinforced concrete beams strengthened by steel reinforced polymer and grout (SRP and SRG) composites", *Mater. Sci. Eng. A*, **412**(1-2), 129-136.

Bonacci, J.F. and Maalej, M. (2001), "Behavioral trends of RC beams strengthened with externally bonded FRP", *J. Compos. Constr.*, **5**(2), 102-103.

Casadei, P., Nanni, A. and Alkhrdaji, T. (2005a), "Steel-reinforced polymer: An innovative and promising material for strengthening infrastructures", *Concr. Eng. Int.*, **9**(1), 54-56.

Casadei, P., Nanni, A., Alkhrdaji, T. and Thomas, J. (2005b), "Performance of double-T prestressed concrete beams strengthened with steel reinforcement polymer", *Adv. Struct. Eng.*, **8**(4), 427-441.

Ceroni, F. and Pecce, M. (2007), "Cracking behaviour of RC beams externally strengthened with emerging

materials", *Constr. Build. Mater.*, **21**(4), 736-745.
Foden, A.J., Balaguru, P., Lyon, R.E. and Davidovits, J. (1997), "Flexural fatigue properties of an inorganic matrix-carbon fiber composite", International SAMPE Symposium and Exhibition (Proceedings), Anaheim, CA, USA, 1345-1354.
Garon, R., Balaguru, P.N., Cao, Y. and Lee, K.-W.W. (2000), "Use of fiber reinforced composites to improve the durability of bridge elements", *Proc. SPIE, Int. Society Opt. Eng.*, **3988**, 440-449.
Giancaspro, J., Balaguru, P. and Lyon, R. (2001), "Hybrid composites with glass/carbon fibers and inorganic/organic matrices", *International SAMPE Symposium and Exhibition (Proceedings),* Long Beach, CA, USA, 2582-2592.
Giancaspro, J., Balaguru, P. and Lyon, R. (2004), "Fire protection of flammable materials utilizing geopolymer", *SAMPE J.*, **40**(5), 42-49.
Giancaspro, J., Lyon, R. and Balaguru, P. (2002), "Flexural behavior of balsa wood cores reinforced with inorganic carbon composite", *International SAMPE Symposium and Exhibition (Proceedings),* Long Beach, CA, United States, 530-541.
Grace, N.F. and Abdel-Sayed, G. (1996), "Double tee and CFRP/GFRP bridge system", *Concr. Int.*, **18**(2), 39-44.
Hammell, J., Balaguru, P. and Lyon, R. (1998), "Influence of reinforcement types on the flexural properties of geopolymer composites", *International SAMPE Symposium and Exhibition (Proceedings)*, Anaheim, CA, USA, 1600-1608.
Harrison, R.R., Rasheed, H.A., Peterman, R.J. and Alkhrdaji, T. (2006), "Comparison of four techniques for strengthening concrete beams using performance and practicality criteria", St. Louis, MO, United States, 70.
Hognestad, E. (1951), "A study of combined bending and axial load in reinforced concrete members", Univ. of Illinois, USA.
Huang, X., Birman, V., Nanni, A. and Tunis, G. (2005), "Properties and potential for application of steel reinforced polymer and steel reinforced grout composites", *Compos. Part B: Eng.*, **36**(1), 73-82.
Karayannis, C.G. and Chalioris, C.E. (2003), "Experimental investigation of the contribution of bonded C-FRP jackets to shear capacity of RC beams", Dundee, United Kingdom, 689-696.
Kim, Y.J., Fam, A., Kong, A. and El-Hacha, R. (2005), "Flexural strengthening of RC beams using steel reinforced polymer (SRP) composites", *7th International Symposium on Fiber-Reinforced (FRP) Polymer Reinforcement for Concrete Structures*.
Kurtz, S. and Balaguru, P. (2001), "Comparison of inorganic and organic matrices for strengthening of RC beams with carbon sheets", *J. Struct. Eng.*, **127**(1), 35-42.
Lopez, A., Galati, N., Alkhrdaji, T. and Nanni, A. (2007), "Strengthening of a reinforced concrete bridge with externally bonded steel reinforced polymer (SRP)", *Compos. Part B: Eng.*, **38**(4), 429-436.
Lyon, R.E., Balaguru, P.N., Foden, A., Sorathia, U., Davidovits, J. and Davidovics, M. (1997), "Fire-resistant aluminosilicate composites", *Fire Mater.*, **21**(2), 67-73.
Masmoudi, R., Theriault, M. and Benmokrane, B. (1998), "Flexural behavior of concrete beams reinforced with deformed fiber reinforced plastic reinforcing rods", *ACI Struct. J.*, **95**(6), 665-675.
Mirmiran, A., Shahawy, M. and Samaan, M. (1999), "Strength and ductility of hybrid FRP-concrete beam-columns", *J. Struct. Eng.*, **125**(10), 1085-1093.
Nanni, A. (1993), "Flexural behavior and design of RC members using FRP reinforcement", *J. Struct. Eng.*, **119**(11), 3344-3359.
Nanni, A. (1997), "CFRP strengthening", *Concr. Int.*, **19**(6), 19-23.
Nanni, A. and Gold, W. (1998), "Strengthening of RC flexural members with FRP composites", Maracaibo, Venezuela, 144-154.
Papakonstantinou, C.G., Balaguru, P. and Lyon, R.E. (2001a), "Comparative study of high temperature composites", *Compos. Part B: Eng.*, **32**(8), 637-649.
Papakonstantinou, C.G. and Balaguru, P.N. (2006), "Fire testing of geopolymer based syntactic foams", *International SAMPE Symposium and Exhibition (Proceedings),* Long Beach, CA, United States, 9.
Papakonstantinou, C.G. and Balaguru, P.N. (2007a), "Fatigue behavior of high temperature inorganic matrix composites", *J. Mater. Civil Eng.*, **19**(4), 321-328.
Papakonstantinou, C.G. and Balaguru, P.N. (2007b), "Geopolymer protective coatings for concrete", *International SAMPE Symposium and Exhibition*, Baltimore, MD, United States, 13.

Papakonstantinou, C.G., Balaguru, P.N. and Lyon, R.E. (2002a), "Hybrid composite panels with fireproof lightweight core and carbon fiber skin", *International SAMPE Symposium and Exhibition (Proceedings)*, Long Beach, CA, United States, 1011-1021.

Papakonstantinou, C.G., Balaguru, P.N. and Petrou, M.F. (2002b), "Analysis of reinforced concrete beams strengthened with composites subjected to fatigue loading", *ACI Special Publication*, **206**(3), 41-60.

Papakonstantinou, C.G., Petrou, M.F. and Harries, K.A. (2001b), "Fatigue behavior of RC beams strengthened with GFRP sheets", *J. Compos. Constr.*, **5**(4), 246-253.

Pecce, M., Ceroni, F., Prota, A. and Manfredi, G. (2006), "Response prediction of RC beams externally bonded with steel-reinforced polymers", *J. Compos. Constr.*, **10**(3), 195-203.

Prota, A., Kah Yong, T., Nanni, A., Pecce, M. and Manfredi, G. (2006), "Performance of shallow reinforced concrete beams with externally bonded steel-reinforced polymer", *ACI Struct. J.*, **103**(2), 163-170.

Saadatmanesh, H. and Malek, A.M. (1998), "Design guidelines for flexural strengthening of RC beams with FRP plates", *J. Compos. Constr.*, **2**(4), 158-164.

Shahawy, M. and Beitelman, T.E. (1999), "Static and fatigue performance of RC beams strengthened with CFRP laminates", *J. Struct. Eng.*, **125**(6), 613-621.

Sharif, A., Al-Sulaimani, G.J., Basunbul, I.A., Baluch, M.H. and Ghaleb, B.N. (1994), "Strengthening of initially loaded reinforced concrete beams using FRP plates", *ACI Struct. J.*, **91**(2), 160-168.

Toutanji, H., Deng, Y., Zhang, Y., Jia, M. and Balaguru, P. (2002), "Static and fatigue performances of RC beams strengthened with carbon fiber sheets bonded by inorganic matrix", *International SAMPE Symposium and Exhibition (Proceedings)*, Long Beach, CA, United States, 1354-1367.

Triantafillou, T.C. and Antonopoulos, C.P. (2000), "Design of concrete flexural members strengthened in shear with FRP", *J. Compos. Constr.*, **4**(4), 198-205.

Tsonos, A.G. (2002), "Seismic repair of exterior R/C beam-to-column joints using two-sided and three-sided jackets", *Struct. Eng. Mech.*, **13**(1), 17-34.

Tsonos, A.G. (2004), "Improvement of the earthquake resistance of R/C beam-column joints under the influence of P-Δ effect and axial force variations using inclined bars", *Struct. Eng. Mech.*, **18**(4), 389-410.

Tsonos, A.G. (2007), "Cyclic load behavior of reinforced concrete beam-column subassemblages of modern structures", *ACI Struct. J.*, **104**(4), 468-478.

Vecchio, F.J. and Collins, M.P. (1986), "Modified compression-field theory for reinforced concrete elements subjected to shear", *J. Am. Concr. Ins.*, **83**(2), 219-231.

Wobbe, E., Silva, P., Barton, B.L., Dharani, L.R., Birman, V., Nanni, A., Alkhrdaji, T., Thomas, J. and Tunis, G. (2004), "Flexural capacity of RC beams externally bonded with SRP and SRG", *International SAMPE Symposium and Exhibition (Proceedings),* Long Beach, CA, United States, 2995-3002.

Youm, K.S., Lee, H.E. and Choi, S. (2006), "Seismic performance of repaired RC columns", *Mag. Concrete Res.*, **58**(5), 267-276.

Appendix: Numerical example

The numerical example presented here deals with a strengthened reinforced concrete beam similar to RB3. More specifically, a RC beam with a span of 1067 mm subjected to four point bending. The cross section of the beam is 100 × 150 mm. The beam is strengthened with steel reinforced inorganic polymer system on the tensile face. The calculation presented here will be for a random concrete strain of $\varepsilon_{cm} = 0.00075$. The basic unknown is c, which will be calculated by the force equilibrium equation.

Initially one needs to calculate the reduced strength of the concrete, f_c'':

$f_c' = 25\text{MPa}$. So: $f_c'' = k \cdot f_c' = 0.92 \cdot 25 = 23\text{MPa}$

The modulus of elasticity is $.E_c(\text{psi}) = 4780 \cdot \sqrt{f_c'} = 4780 \cdot \sqrt{25} = 23.9\text{GPa}$.

From Eq. (11):

$$f_c = f_c'' \cdot \left[2\frac{\varepsilon_{cm}}{\varepsilon_o} - \left(\frac{\varepsilon_{cm}}{\varepsilon_o}\right)^2\right] = 23 \cdot \left[2\frac{0.0008}{0.0018} - \left(\frac{0.0008}{0.0018}\right)^2\right] = 15.9\text{MPa}$$

$$\varepsilon_o = 2\frac{f_c''}{E_c} = 2\frac{k \cdot 23}{23900} = 2\frac{0.92 \cdot 23}{23900} = 0.0018$$

from Eq. (13): $\alpha = \dfrac{\int_0^{\varepsilon_{cn}} f_c d\varepsilon_c}{f_c'' \varepsilon_m} = 0.162$

from Eq. (16): $\gamma = \dfrac{\int_0^{\varepsilon_{cn}} \varepsilon_c f_c d\varepsilon_c}{\varepsilon_m \cdot \int_0^{\varepsilon_{cn}} f_c d\varepsilon_c} = 0.653$

from Eq. (17) the tensile strength is $f_{ct} = \dfrac{\alpha_1 \cdot \alpha_2 \cdot f_{cr}}{1 + \sqrt{500\varepsilon_{cm}}} = \dfrac{0.7 \cdot 1 \cdot 3.14}{1 + \sqrt{500 \cdot 0.0008}} = 1.35\text{MPa}$

and $f_{cr} = 0.7\sqrt{f_c'}$

The location of the neutral axis can be determined using Eq. (18):

$$\alpha \cdot f_c'' \cdot b \cdot c + \sum_{i=1}^{n} f_{si}A_{si} + f_f A_f + f_{ct} b\frac{d-c}{2} = 0$$

$$\Rightarrow 0.162 \cdot 21.16 \cdot 100 \cdot c + 200000 \cdot 0.0008\left(\frac{c-133}{c} + \frac{c-17}{c}\right) \cdot 63 + 193100 \cdot 0.0008\left(\frac{c-151.5}{c}\right) \cdot 32$$

$$- 1.35 \cdot 100\frac{150-c}{2} = 0$$

$$\Rightarrow c = 58.19\text{mm}$$

From Eq. (19) the moment can be calculated:

$$M = \alpha \cdot f_c'' \cdot b \cdot c\left(\frac{h}{2} - \gamma c\right) + \sum_{i=1}^{n} f_{si}A_{si}\left(\frac{h}{2} - d_i\right) + f_f A_f\left(\frac{h}{2} - d_f\right) + f_{ct} b\frac{2(h-c)}{3}\frac{d-c}{2}$$

$$M = 0.162 \cdot 21.16 \cdot 100 \cdot 58.19 \cdot \left(\frac{150}{2} - 0.653 \cdot 58.19\right) + (-12959) \cdot \left(\frac{150}{2} - 133\right) + 7135 \cdot \left(\frac{150}{2} - 12.7\right)$$

$$+ (7927) \cdot \left(\frac{150}{2} - 151.5\right) + 6197\frac{2(150-58.19)}{3}$$

$$M = 19947 \cdot 37 + (-12959) \cdot (-58) + 7135 \cdot 62.3 + (-7927) \cdot (-76.5) + 6197 \cdot 61.2$$

$$M = 2{,}919{,}938\text{Nmm}$$

$$Form \xrightarrow{eq.22} P = \frac{6 \cdot M}{L} = \frac{6 \cdot 2{,}919{,}938}{1067} = 16{,}419.5N$$

the curvature from Eq. (20) is: $\phi = \frac{0.0008}{58.19} = 1.37 \cdot 10^{-5}$

Using the curvature, from Eq. (23) the mid-span deflection can finally be calculated:

$$\Delta = \frac{\phi L^2}{9.39} = \frac{1.37 \cdot 10^{-5} \cdot 1067^2}{9.39} = 1.67\text{mm}$$

Notation

b	beam width
h	beam height
f_c	compressive strength of concrete (in stress strain graph)
f_c'	compressive strength of concrete at 28 days determined using cylinders
f_c''	reduced compressive strength of concrete
k	factor used to reduce the compressive strength
E_c	modulus of elasticity of concrete
E_{si}	modulus of elasticity of tensile reinforcing steel
E_f	modulus of elasticity of FRP sheet
ε_{cm}	concrete strain, in top compressive face
ε_{si}	strain of tensile reinforcing steel
ε_f	strain of steel fibers
c	distance of the neutral axis from the top flange
f_{si}	stress in tensile reinforcing steel
f_f	stress in FRP sheet
f_y	yielding stress of tensile reinforcing steel
A_{si}	cross sectional area of reinforcing steel
A_f	cross sectional area of FRP sheet
C_c	concrete compression force
S_i	tensile reinforcing steel tension force
P_f	FRP sheet tension force
A	area under the stress strain curve of concrete
d_{si}	distance of steel flexural reinforcement from top flange
d_f	distance of FRP sheet from top flange
ε_{cr}	strain of concrete at cracking
α_1	factor accounting for bond characteristics of reinforcement
α_2	factor accounting for sustained or repeated loading respectively
f_{cr}	stress in concrete when cracking occurs
f_{ct}	tensile capacity of concrete after cracking
φ	curvature at midspan
Δ	deflection at midspan
P	applied load
M	maximum moment
L	span length